



Investigation on behaviors of acoustoelastic cavities using a novel reduced finite element–dual reciprocity boundary element formulation

Wei Liu, Saeed Bornassi, Yedan Shen, Mohammad Ghalandari, Hassan Haddadpour, Rohollah Dehghani Firouzabadi, Shahab S. Band & Kwok-wing Chau

To cite this article: Wei Liu, Saeed Bornassi, Yedan Shen, Mohammad Ghalandari, Hassan Haddadpour, Rohollah Dehghani Firouzabadi, Shahab S. Band & Kwok-wing Chau (2021) Investigation on behaviors of acoustoelastic cavities using a novel reduced finite element–dual reciprocity boundary element formulation, *Engineering Applications of Computational Fluid Mechanics*, 15:1, 1885–1901, DOI: [10.1080/19942060.2021.1996464](https://doi.org/10.1080/19942060.2021.1996464)

To link to this article: <https://doi.org/10.1080/19942060.2021.1996464>



© 2021 The Author(s). Published by Informa UK Limited, trading as Taylor & Francis Group



Published online: 23 Nov 2021.



[Submit your article to this journal](#)



Article views: 1094



[View related articles](#)



[View Crossmark data](#)



Citing articles: 1 [View citing articles](#)

Investigation on behaviors of acoustoelastic cavities using a novel reduced finite element–dual reciprocity boundary element formulation

Wei Liu^a, Saeed Bornassi^b, Yedan Shen^c, Mohammad Ghalandari^b, Hassan Haddadpour^b, Rohollah Dehghani Firouzabadi^b, Shahab S. Band^{b,d} and Kwok-wing Chau^{b,e}

^aSchool of Economics and Commerce, Guangdong University of Technology, Guangzhou, People's Republic of China; ^bDepartment of Aerospace Engineering, Sharif University of Technology, Tehran, Iran; ^cSchool of Mathematics and Information Sciences, Guangzhou University, Guangzhou, People's Republic of China; ^dFuture Technology Research Center, College of Future, National Yunlin University of Science and Technology, 123 University Road, Section 3, Douliou, Yunlin 64002, Taiwan, People's Republic of China; ^eDepartments of Civil and Environmental Engineering, Hong Kong Polytechnic University, Hong Kong, People's Republic of China

ABSTRACT

This paper presents the acoustic and structure characteristics of chambers with elastic/rigid baffles and elastic walls using a novel formulation. The acoustic fluid is assumed to be compressible and inviscid, and the effect of mean flow is neglected. The acoustic field is formulated based on the dual reciprocity boundary element method (DRBEM), and the finite element method (FEM) is used to model the structural dynamics of elastic walls. The reduced-order model (ROM) of the coupled system is derived based on modal analysis of the acoustic field with rigid boundaries and the structure in a vacuum. Numerical examples are presented, and the acoustic modes and frequencies of the chambers are determined by analysis of eigenvalues of the coupled governing equations. The accuracy of the introduced model, which is based on the reduced-order DRBEM-FEM formulation, is examined by comparing the results with analytical and numerical predictions reported in the literature, and good agreements are achieved. Besides, the effects of baffles are studied for different configurations and the elasticity of a wall in a combustion chamber is investigated.

ARTICLE HISTORY

Received 8 April 2021
Accepted 14 October 2021

KEYWORDS




acoustoelastic; dual reciprocity boundary element method; finite element method; baffled structures

1. Introduction

The interaction between acoustic waves and solid structures is a field of interest in fluid–structure interaction (FSI) dynamics (L. Chen et al., 2020; Ghalandari, Bornassi, et al., 2019; Ghalandari, Shamshirband, et al., 2019; Ghalandari, Ziamolki, et al., 2019; Zeinalzadeh & Pakatchian, 2021). These fields of FSI problems have been challenging areas in many engineering applications, such as high-frequency instability and humming of combustion chambers in fluid fuel engines (Anderson & Yang, 1995). Reviews of numerical solutions in low-frequency structure–acoustic problems, with an emphasis on the most popular state-of-the-art methods, have been presented in several research studies (Atalla & Bernhard, 1994; Li et al., 2021; Shu et al., 2012; D. Zhao & Li, 2015). Acoustic resonance in the chamber domain is the main cause of instabilities. Taciturnity of flame, blowout (Hussin et al., 2021), humming and hydrodynamic acoustic forces exerted on the walls of the chambers, which may damage the entire structures of combustion, are considered to account for 90% of destructive results of the

acoustic problem (Ar'kov et al., 1972; Iurashev et al., 2017; Sui et al., 2021). Radial baffles, which are used at the interfaces of the injector, are considered as common solution techniques for controlling acoustic resonance, especially in modified premixed combustion chambers (Hambric et al., 2016; Han et al., 2021). Dissipation of acoustic energy and increasing damping effects by 30% can decrease the intensity of acoustic resonance in combustion chambers (Baer & Mitchell, 1977) by about 40%. The characteristic effects of these components on the nozzle of a combustion chamber were studied by Farshchi et al. (2009). They showed that the converged nozzle had a great influence on longitudinal and tangential modes. Wieber (1966) experimentally studied the effects of a radial baffle on a cold acoustic combustion chamber. Later, Webster et al. (2017) experimentally conducted both cold and hot firing tests and reported the consequences of the configuration of a radial baffle on damping under both tangential and longitudinal modes.

Investigations on the dynamic properties of such applied problems by the valuable numerical method

CONTACT Yedan Shen  yedanshentrina@sina.com; Mohammad Ghalandari  Ghalandary.13518@gmail.com; Shahab S. Band  shamshirbands@yuntech.edu.tw

have become prevalent in recent years. The finite difference, finite volume, finite element (FEM) and boundary element (BEM) methods (Brebbia & Dominguez, 1994) have been commonly utilized by many researchers. Among these methods, the BEM, by representing its inherent mesh features, is efficient and convenient for acoustic problems. Indeed, meshing the boundary instead of the entire domain is the principal advantage of BEM, as it decreases the size of equations and subsequently saves computational cost and time (Firouz-Abadi et al., 2008). Several BEMs to investigate the analysis of eigenvalues in Helmholtz problems were presented by Kamiya et al. (1993) and Ali et al. (1995). The multiple reciprocity method (MRM) and dual reciprocity method (DRM) (Fahmy, 2018; Yu et al., 2021) have provided an interesting application of BEMs, especially in the simulation of Helmholtz equations. Kontoni et al. (1991), Sladek et al. (1993) and W. Zhao et al. (2019) used these techniques in the eigenvalue analysis of acoustic problems in two- and three-dimensional fluid domains. The isogeometric BEM is a new and thriving approach for tackling acoustic problems with the same basic traditional BEM phenomena (L. L. Chen et al., 2019; Dölz et al., 2018; Simpson et al., 2014).

The FEM model is another useful robust method which was used for acoustic applications in the late 1960s by Gladwell and Zimmermann (1966). In contrast to the symmetric and sparse features of FEM matrices, the BEM formulation suffers from fully populated and asymmetric matrices. Indeed, the FEM formulation was derived based on the variational technique for a specific acoustic problem. Later, Craggs (1972) studied the natural properties and mode shape of acoustic inclusions using an FEM model. Kim et al. (2015) assessed the stability of a combustion chamber using the FEM and showed a maximum of 1% error difference between their results and the analytical solution.

To take the advantage of both the FEM and BEM in fluid–structure problems, some researchers (Gaul & Wenzel, 2002; Junge et al., 2011) have been motivated to use a combination of both methods simultaneously. Despite this, there remains a need to reduce both the size of equations and the computational effort, and methods based on reduced-order techniques have received a lot of attention recently (Gonzalez-Flesca et al., 2018). Ohayon (2001) and Ohayon and Soize (2012) proposed several variational formulations for the modal analysis of bounded fluid–structure systems to investigate internal vibration–acoustic and hydroelastic systems. The application of modal synthesis for combined structure–acoustic systems was used by Wolf (1976) to determine the low-frequency free and forced interior acoustic properties of passenger compartments. An investigation

on vibrational behavior of the acoustic–structure problem using an isogeometric BEM was conducted using the directed coupling method and symmetric–iterative coupling method (Wu et al., 2020). This approach was shown to have low accuracy near the natural frequency of the structure.

Although there are some limitations in the modeling and solution of fluid by the FEM and structures using the BEM, a novel efficient reduced-order FEM-BEM model for the treatment of the acoustic instability of chambers using elastic baffles and walls is presented. To derive the governing equation of the acoustic medium, the fluid is assumed to be homogeneous, isotropic, inviscid and compressible, and the effect of mean flow is neglected. Using the dual reciprocity boundary element method (DRBEM), the equation of the acoustic domain is introduced to the elastic structure. The reduced-order model of elastic structure is obtained via modal analysis using the FEM technique. The reduction of computational cost by the BEM and the robustness of the FEM approach are the main advantages of this formulation model, which is a novel technique for the solution of real problems with the lowest computational cost for this type of problem (Gonzalez-Flesca et al., 2018; W. Zhao et al., 2019). Indeed, a challenging part of this study that arises from the BEM in the solution of rigid and elastic baffled structures is solved by the zoning method, which enables the BEM to approximate the acoustic characteristics of cavities with baffles. The minimum differences between the results and those from the literature prove the capability of the proposed model to solve interactive coupled problems in different forms of cavities.

2. Structure domain

In this paper, the FEM is used to model the structural dynamics of the system. The flexible structure is modeled by beam or shell elements. Neglecting damping, the FEM formulation of structural dynamics can be expressed as:

$$\mathbf{M}_s \ddot{\mathbf{d}} + \mathbf{K}_s \mathbf{d} = \mathbf{f} \quad (1)$$

where \mathbf{M}_s and \mathbf{K}_s represent the mass and stiffness matrices, respectively. \mathbf{d} is the vector of nodal displacements and \mathbf{f} denotes the external nodal force vector.

Reduced-order models (ROMs) of the structure domain can be constructed using the modal analysis technique. The motion of the structure can be described by an expansion of the structural displacement as a reduced set of basis vectors, expressed as

$$\mathbf{d} = \sum_{i=1}^{N_s} \boldsymbol{\psi}_i \xi_i(t) = \boldsymbol{\Psi} \boldsymbol{\xi} \quad (2)$$

where N_s is the number of modes, Ψ is a matrix with mass-normalized mode shapes in the columns and ξ is a vector containing the corresponding modal coordinates. By substituting Equation (2) into Equation (1), pre-multiplying by Ψ^T and using the orthogonality of mode shapes, the governing equations are reduced to a set of uncoupled equations, as

$$\mathbf{I}\ddot{\xi} + \mathbf{\Omega}_s\xi = \mathbf{R} = \Psi^T\mathbf{f} \quad (3)$$

where \mathbf{I} is an identity matrix and $\mathbf{\Omega}_s$ is a diagonal matrix whose elements are squares of natural frequencies. A few modes can be used to construct the ROM of the structure by suppressing higher frequency modes. Thus, the number of mode shapes used to describe the vibration of the structure is much smaller than the degrees of freedom of the complete system. Using the ROM technique, the size of the equations decreases considerably, and computational cost and time are significantly improved (Gonzalez-Flesca et al., 2018). Vector \mathbf{R} denotes generalized forces equivalent to work done by external forces at each mode shape. In the absence of body and other external forces, the pressure of acoustic waves (p) is the prominent source of excitation. Thus, the resulting generalized forces can be expressed as

$$\mathbf{R}_i = \int_s p \psi_i^n dS \quad (4)$$

where ψ_i^n is the normal displacement of the i th mode shape and can be computed by projecting mode shapes along the normal direction outward from the surface (S).

3. Acoustic domain

In this section, the BEM formulation of the acoustic domain is presented and then the ROM of the equations is introduced based on the modal analysis technique.

To derive the governing equations of the acoustic field, the fluid is assumed to be homogeneous, isotropic and compressible. In addition, the fluid is considered to be irrotational and inviscid. Based on these considerations and assuming infinitesimal fluctuation of pressure, temperature, velocity and density distributions, the continuity and momentum equations in combination with isentropic relationships are reduced to the well-known linear acoustic wave equation. The isentropic equation relating sound pressure and density perturbation is a constitutive equation in the acoustic field. Thus, the linear governing equation of acoustic waves in terms of the velocity potential field (Φ) can be expressed as:

$$\nabla^2 \Phi = \frac{1}{c^2} \frac{\partial^2 \Phi}{\partial t^2} \quad (5)$$

where ∇^2 is the Laplace operator and c is the speed of sound in the media.

In general, there are three types of boundary conditions in the acoustic governing equation and these can be classified as follows.

The velocity potential or pressure:

$$\Phi = \bar{\Phi} \quad (6)$$

The velocity:

$$\frac{\partial \Phi}{\partial \mathbf{n}} = \mathbf{q} \quad (7)$$

The impedance:

$$\mathbf{q} = \frac{\partial \Phi}{\partial \mathbf{n}} = -\frac{\mu}{c} \dot{\Phi} \quad (8)$$

where μ is the absorbent coefficient of the surface, \mathbf{q} is the normal derivative of the velocity potential, which is the normal velocity, and \mathbf{n} is the outward normal direction on the boundary. In this paper, the application of the second type of boundary condition, known as the Neumann boundary condition, is involved.

3.1. Boundary element formulation

Apart from the acoustic wave equation (Equation 5), there exist many other engineering applications in which the governing equations contain Laplacian and other terms:

$$\nabla^2 \Phi = b \quad (9)$$

The term b can be a function of coordinates, the primary variable (Φ) and its time or spatial derivatives.

Using the fundamental solution and by implementation of Green's second identity, one can convert the boundary-value problem (Equation 9), and the corresponding boundary conditions (Equations 6–8) into the boundary integral equations. The basic solution Φ^* for potential problems must satisfy the following Poisson equation:

$$\nabla^2 \Phi^* = \delta(\mathbf{R} - \mathbf{R}_p) \quad (10)$$

where $\delta(\mathbf{R} - \mathbf{R}_p)$ denotes the Dirac delta function, which represents a unit source at the point with the coordinate of $\mathbf{R}_p = x_p \hat{i} + y_p \hat{j} + z_p \hat{k}$, and Φ^* explains the response at the field point $\mathbf{R} = x \hat{i} + y \hat{j} + z \hat{k}$ due to that source. The basic solution Φ^* for three-dimensional problems and its normal derivative are given by:

$$\Phi^* = \frac{1}{4\pi r} \quad (11)$$

$$q^* = \frac{\partial \Phi^*}{\partial \mathbf{n}} = -\frac{\mathbf{r} \cdot \mathbf{n}}{4\pi r^3} \quad (12)$$

where \mathbf{n} is the outward normal vector on the boundary and \mathbf{r} is the vector of the distance between the source

point and field point, and its absolute value is denoted by r .

Applying Green's second identity to the governing equation (Equation 9), the conventional form of the boundary integral formulation is derived as

$$c_p \Phi_p = \int_s (\Phi q^* - q \Phi^*) ds + \int_V (\Phi^* b) dV \quad (13)$$

$$c_p = \frac{\chi}{4\pi} \quad (14)$$

in which χ is a coefficient denoting the internal angle of the source point in radians. If the source point is located on a smooth or flat boundary, c_p is equal to 0.5, and for source points into the field regions, it is equal to 1.

It can be seen that the boundary element formulation of the Poisson equation leads to the conventional form of the boundary integral equation (Equation 13), which consists of two integral parts: one part is the boundary integral and the other is the domain integral part. Such domain integral terms have been a major difficulty in the development of the BEM, which weakens the main advantage of this method. As mentioned in Section 1, dealing with boundary integrals instead of domain integrals and meshing the boundary instead of the internal domain are the main benefits of the BEM compared to other numerical methods such as the FEM. The need to handle domain integrals has motivated many researchers to find solution methods which are general, simple and easy to use. Many solution methods, such as the internal cell method (ICM), particular solution method (PSM), MRM and, more recently, the DRM have been proposed as the result of considerable research efforts. The following subsection explains the outstanding performance of the DRM in addressing the solution of domain integrals as well as boundary integrals.

3.2. Dual reciprocity method (DRM)

The DRM is a treatment for domain integrals which was first introduced for solving acoustic-structure problems. It is an innovative approach to transforming domain integrals into boundary integrals. Based on the PSM, the solution of Equation (13) is the summation of a homogeneous solution with a particular solution $\hat{\Phi}$, which satisfies the following equation:

$$\nabla^2 \hat{\Phi} = b \quad (15)$$

In general, it is difficult to find a particular solution for any type of Poisson equation, especially when the term b is nonlinear and time dependent. However, it is possible to approximate b as a set of basic functions which have

particular solutions as:

$$b \simeq \sum_{j=1}^{N_B+N_I} \alpha_j f_j \quad (16)$$

where α_j denotes undetermined coefficients and f_j is known as the approximating functions, which are geometry dependent (Brebbia & Dominguez, 1994). N_B and N_I are the number of boundary and internal points, respectively.

The relationship between the approximating functions and their corresponding particular solutions is as follows:

$$\nabla^2 \hat{\Phi}_j = f_j \quad (17)$$

Using Equations (15)–(17) and substituting the results into Equation (13) yields:

$$\begin{aligned} c_i \Phi_i + \int_s (\Phi q_i^* - q \Phi_i^*) ds \\ = \sum_{j=1}^{N_B+N_I} \alpha_j \left(\int_V (\Phi_i^* \nabla^2 \hat{\Phi}_j) dV \right) \end{aligned} \quad (18)$$

By applying Green's second identity for the term on the right-hand side of Equation (18), one obtains:

$$\begin{aligned} c_i \Phi_i + \int_s (\Phi q_i^* - q \Phi_i^*) ds \\ = \sum_{j=1}^{N_B+N_I} \alpha_j \left(c_i \hat{\Phi}_{ij} + \int_s (\hat{\Phi}_j q_i^* - \hat{q}_j \Phi_i^*) ds \right) \end{aligned} \quad (19)$$

where \hat{q}_j is analogous to $q = \frac{\partial \Phi}{\partial n}$ and n is the outward normal direction on the boundary. It is observed that there is no domain integral in Equation (19). This boundary integral equation can be solved by discretizing the boundary into small elements. The shape of these elements can be triangular or quadrilateral. By integrating over each boundary element and adding the contribution of all elements, Equation (19) can be written as:

$$\begin{aligned} c_i \Phi_i + \sum_{k=1}^{N_B} \int_{S_K} \Phi q_i^* dS_k - \sum_{k=1}^{N_B} \int_{S_K} q \Phi_i^* dS_k \\ = \sum_{j=1}^{N_B+N_I} \alpha_j \left(c_i \hat{\Phi}_{ij} + \sum_{K=1}^{N_B} \int_{S_K} \hat{\Phi}_j q_i^* dS_k \right. \\ \left. - \sum_{k=1}^{N_B} \int_{S_K} \hat{q}_j \Phi_i^* dS_k \right) \end{aligned} \quad (20)$$

where k is the number of boundary elements. The variation of the unknown variable Φ and q over the elements

can be approximated in terms of their nodal values by introducing appropriate interpolation functions as:

$$\Phi = N_k \Phi_k \quad (21)$$

$$q = N_k q_k \quad (22)$$

where Φ_k and q_k are vectors consisting of nodal values of acoustic potential and normal velocity, respectively, and N_k is a matrix of element interpolation functions. It should be noted that for simplicity and to increase the efficiency of the methods, $\hat{\Phi}$ and \hat{q} , which are known functions, can also be approximate over boundary elements, as well as unknown variables. Inserting Equations (21) and (22) into Equation (20), the boundary integral equation can be expressed as:

$$\begin{aligned} c_i \Phi_i + \sum_{k=1}^{N_B} H_{ik} \Phi_k - \sum_{k=1}^{N_B} G_{ik} q_k \\ = \sum_{j=1}^{N_B+N_I} \alpha_j \left(c_i \hat{\Phi}_{ij} + \sum_{k=1}^{N_B} H_{ik} \hat{\Phi}_{kj} - \sum_{k=1}^{N_B} G_{ik} \hat{q}_{kj} \right) \end{aligned} \quad (23)$$

in which

$$H_{ik} = \int_{S_K} q_i^* N_k dS_k \quad (24)$$

$$G_{ik} = \int_{S_K} \Phi_i^* N_k dS_k \quad (25)$$

By representing the above integrals in the local coordinate systems of elements, they can be evaluated numerically by the Gauss quadrature method. Employing Equation (23) for all boundary and internal points by using point collocation techniques, a set of linear algebraic equations is obtained:

$$H\Phi - Gq = (H\hat{U} - G\hat{Q})\alpha \quad (26)$$

The terms c_i are incorporated into the diagonal terms of the matrix H . The unknown coefficient vector α can be obtained by evaluating the term b at $N_B + N_I$ points, which may be written in matrix form as:

$$b = F\alpha \quad (27)$$

Each column of the matrix F consists of approximate functions f_j at $N_B + N_I$ collocation points. By obtaining α from the previous equation and substituting the result into Equation (26), one derives:

$$H\Phi - Gq = (H\hat{U} - G\hat{Q})F^{-1}b \quad (28)$$

where Φ and q are vectors containing nodal values of acoustic potential and normal velocity at the walls, entire boundary and internal collocation points.

In the acoustic wave equation, b is equal to a time-dependent inertia term. Finally, by replacing the inertia

term in Equation (28), the DRM-based BEM formulation of the acoustic domain with baffles can be written as:

$$M_f \begin{bmatrix} \ddot{\Phi}_{wall} \\ \ddot{\Phi}_{interface} \\ \ddot{\Phi}_{domain} \end{bmatrix} + K_f \begin{bmatrix} \Phi_{wall} \\ \Phi_{interface} \\ \Phi_{domain} \end{bmatrix} = G \begin{bmatrix} q_{wall} \\ q_{interface} \\ q_{domain} \end{bmatrix} \quad (29)$$

in which

$$M_f = -\frac{1}{c^2} (H\hat{U} - G\hat{Q})F^{-1} \quad (30)$$

$$K_f = H \quad (31)$$

where M_f and K_f are the acoustic mass and stiffness matrices, respectively. They are composed of submatrices corresponding to the walls, boundary and internal points, and have a size of $N_B + N_I$. \hat{U}_s and \hat{Q} are matrices whose columns are a vector of particular solutions and their normal derivative at $N_B + N_I$ points, respectively. Since the value of \hat{q} at internal points is meaningless, the corresponding value of \hat{q} in matrix \hat{Q} is zero. According to the mass conservation law, q values at the inlet and outlet of the interface are equal. Besides, the potential values at the interface and the entire domain are equal.

One of the most important considerations influencing the accuracy of DRM results is the choice of appropriate approximate functions f . Many types of approximate functions have been proposed, but radial-based functions (Bebbia & Dominguez, 1994) are the simplest and most accurate.

$$f = 1 + r + r^2 + \dots \quad (32)$$

The corresponding particular solutions and normal derivatives become:

$$\hat{\Phi} = \frac{r^2}{4} + \frac{r^3}{9} + \frac{r^4}{16} + \dots \quad (33)$$

$$\hat{q} = \left(\frac{1}{2} + \frac{r}{3} + \frac{r^2}{4} + \dots \right) r.n \quad (34)$$

According to the results reported in the literature, choosing the first two terms of f and the resulting $\hat{\Phi}$ and \hat{q} functions will provide the most accurate alternatives. The accuracy of the DRM results also depends on the number of internal points and, consequently, the number of approximating functions that are used for the expansion of b . Although there exist rare cases in which the solutions are sensitive to the number of internal points, the convergence of results in terms of the number of internal points is accomplished in this paper as well.

3.3. Reduced order model

To derive the ROM of the acoustic equation, the velocity potential is expressed in terms of acoustic mode shapes in

a closed cavity with rigid walls. The solution of the acoustic equation is assumed to be harmonic and is given as:

$$\Phi = \bar{\Phi} e^{i\omega t} \quad (35)$$

Substituting Equation (35) into Equation (29) and applying the boundary conditions ($\mathbf{q} = 0$) yields standard eigenvalue problems, which can be used to determine acoustic natural frequencies and the corresponding mode shapes. The right and left eigenvalue problems are as follows:

$$\mathbf{K}_f \bar{\Phi}_i^r = \bar{\lambda}_i \mathbf{M}_f \bar{\Phi}_i^r \quad (36)$$

$$\mathbf{K}_f^T \bar{\Phi}_i^l = \bar{\lambda}_i \mathbf{M}_f^T \bar{\Phi}_i^l \quad (37)$$

where $\bar{\lambda}_i = \omega_i^2$ is the i th eigenvalue, and $\bar{\Phi}_i^r$ and $\bar{\Phi}_i^l$ are, respectively, the i th right and left eigenvectors, which are bi-orthogonal with respect to the mass and stiffness matrices. By considering all eigenvectors, one can obtain:

$$\mathbf{Y}^T \mathbf{M}_f \mathbf{X} = \mathbf{I}$$

$$\mathbf{Y}^T \mathbf{K}_f \mathbf{X} = \boldsymbol{\Omega}_f \quad (38)$$

where $\boldsymbol{\Omega}_f$ is a matrix with the square of natural frequencies in the diagonal. Matrices \mathbf{X} and \mathbf{Y} contain columns of the right and left eigenvectors, respectively.

The solution of Equation (29) is assumed to be given by a linear combination of the right eigenvectors as:

$$\Phi \simeq \sum_{i=1}^{N_f} \bar{\Phi}_i^r \eta_i(t) = \mathbf{X} \boldsymbol{\eta} \quad (39)$$

where N_f is the number of acoustic mode shapes and η_i denotes the generalized modal coordinates. By substituting Equation (39) into Equation (29), pre-multiplying with \mathbf{Y}^T and using bi-orthogonality relationships, the equations are reduced to:

$$\mathbf{I} \ddot{\boldsymbol{\eta}} + \boldsymbol{\Omega}_f \boldsymbol{\eta} = \mathbf{Y}^T \mathbf{G} \mathbf{q} \quad (40)$$

4. Coupled domain

The reduced model of the coupled system can be obtained based on the ROM of each structure or fluid subdomain. This aim is accomplished by solving the structural problem *in vacuo* (in the absence of acoustic fluid) and the acoustic subdomain with rigid boundaries.

In the structure subdomain, generalized structural forces due to acoustic pressure can be computed with other boundary integrals over the entire surface. Therefore, by approximating the pressure $\mathbf{p} = \mathbf{N}_k \mathbf{p}_k$ within

each boundary element and performing the integration over the boundary mesh, one obtains:

$$\mathbf{R}_i = \int_s \mathbf{p} \psi_i^n dS = \sum_{k=1}^{N_B} \mathbf{W}_{ik} \mathbf{p}_k \quad (41)$$

in which

$$\mathbf{W}_{ik} = \int_s \psi_i^n \mathbf{N}_k dS_k \quad (42)$$

By substituting Equation (41) into Equation (3) and using the linearized unsteady Bernoulli's equation ($\mathbf{p} = -\rho \dot{\Phi}$), the equation for the structure can be expressed as:

$$\mathbf{I} \ddot{\boldsymbol{\xi}} + \boldsymbol{\Omega}_f \boldsymbol{\xi} = \mathbf{W}_p = -\rho \mathbf{W} \dot{\Phi} \quad (43)$$

Substituting the acoustic potential expansion (Equation 39) into this equation yields:

$$\mathbf{I} \ddot{\boldsymbol{\xi}} + \boldsymbol{\Omega}_f \boldsymbol{\xi} = -\rho \mathbf{W} \mathbf{X} \dot{\boldsymbol{\eta}} \quad (44)$$

In the interaction of acoustic fluid and structure at the boundary, fluid particles and structure move together, which is known as the continuity of displacement field at the interface. Using the continuity condition, the acoustic fluid velocity vector in the normal direction (\mathbf{q}) can be computed by taking the time derivative of the structure normal displacement (\mathbf{d}^n), namely:

$$\mathbf{q} = \dot{\mathbf{d}}^n = \mathbf{T} \dot{\boldsymbol{\xi}} \quad (45)$$

By substituting Equation (45) into the acoustic equation (Equation 40), one obtains:

$$\mathbf{I} \ddot{\boldsymbol{\eta}} + \boldsymbol{\Omega}_f \boldsymbol{\eta} = \mathbf{Y}^T \mathbf{G} \mathbf{T} \dot{\boldsymbol{\xi}} \quad (46)$$

where \mathbf{T} is a matrix whose columns are structure mode shapes projected in the normal direction. Finally, by combining Equations (44) and (46), the ROM of the coupled system can be written as:

$$\begin{bmatrix} \mathbf{I} & 0 \\ 0 & \mathbf{I} \end{bmatrix} \begin{bmatrix} \ddot{\boldsymbol{\xi}} \\ \ddot{\boldsymbol{\eta}} \end{bmatrix} + \begin{bmatrix} 0 & \mathbf{C}_{sf} \\ \mathbf{C}_{fs} & 0 \end{bmatrix} \begin{bmatrix} \dot{\boldsymbol{\xi}} \\ \dot{\boldsymbol{\eta}} \end{bmatrix} + \begin{bmatrix} \boldsymbol{\Omega}_s & 0 \\ 0 & \boldsymbol{\Omega}_f \end{bmatrix} \begin{bmatrix} \boldsymbol{\xi} \\ \boldsymbol{\eta} \end{bmatrix} = \begin{bmatrix} 0 \\ 0 \end{bmatrix} \quad (47)$$

in which:

$$\mathbf{C}_{sf} = \rho \mathbf{W} \mathbf{X} \quad (48)$$

5. Results and discussion

Based on the presented formulation (DRBEM-FEM), some test cases (Farshchi et al., 2009; Laudien et al., 1995; Wieber, 1966) are studied in this section and are compared with FEM simulation and analytical results.

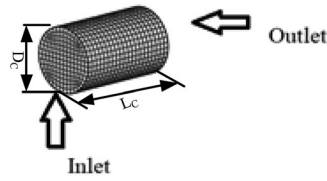


Figure 1. Three-dimensional mesh of the chamber.

Table 1. Mean error in first natural frequencies for a rigid cylinder with respect to internal mesh points.

Mesh type	N_I/N_B	Error (%)
1	0	1.8
2	0.2	0.4
3	0.5	0.31
4	1	0.26

Besides, the formulation is examined for cylindrical geometry and for a nozzle combustion chamber filled with air ($\rho_f = 1.21 \text{ kg/m}^3$, $c = 343 \text{ m/s}$) by determining their acoustic modal parameters. The investigations are followed by rigid baffled cavities for both cylindrical and nozzle geometries. The effects of flexibility of the baffles on the acoustic characteristics of nozzle combustion are also presented. Furthermore, an axisymmetric cavity filled by another fluid ($\rho_f = 565 \text{ kg/m}^3$ and $c = 730 \text{ m/s}$) is adopted to study the effect of elasticity of steel walls on the acoustic domain by the proposed formulation.

5.1. Cylindrical combustion chamber

The first test case is a rigid cylindrical chamber (Figure 1) with a length (L_C) of 53 cm and a diameter (D_C) of 34 cm. The domain is discretized by 20 shell elements in the longitudinal direction, seven shell elements in the radial direction and 40 shell elements in the circumferential direction. A sensitivity analysis of results with respect to the number of internal collocation points chosen in the DRM is established to ensure the accuracy and efficiency of the method. The accuracy of the introduced formulation is evaluated for chambers with closed-end boundary conditions.

The results of a mesh study on the first 18 natural frequencies of the cavity for the corresponding mesh, with respect to the variation of the number of internal points to boundary points (N_I/N_B), are presented in Table 1.

Based on the mesh sensitivity analysis of a cylinder in the literature (Farshchi et al., 2009; Laudien et al., 1995; Wieber, 1966), the accuracy of the numerical results is enhanced with the increase in the number of internal points with uniform distribution, and is acceptable for $\frac{N_I}{N_B} > 0.2$.

A comparison of the results for the first 18 modes with the FEM and the literature (Farshchi et al., 2009;

Table 2. Comparison of the frequency for a cylinder with closed end.

Mode	Wieber (1966)	Laudien et al. (1995)	FEM	Present
L1	322.40	322.10	321.09	321.91
T1	592.00	590.60	587.80	596.48
L2	644.90	642.20	644.15	643.01
L1T1	674.10	671.20	669.79	665.61
L2T1	875.40	867.90	872.04	869.73
L3	967.30	958.40	971.19	972.84
T2	982.00	974.80	976.78	974.74
L1T2	1033.60	1024.10	1028.23	1022.10
L3T1	1134.10	1117.70	1135.18	1130.75
L2T2	1174.80	1158.30	1170.08	1166.14
R1	1232.50	1215.40	1229.55	1237.76
L1R1	1274.00	1253.90	1270.79	1271.79
L4	1289.70	1268.60	1304.19	1313.32
T3	1350.70	1330.00	1349.49	1340.39
L3T2	1378.40	1349.70	1378.14	1376.05
L1T3	1388.70	1364.80	1387.16	1379.18
L2R1	1391.00	1361.90	1388.05	1400.10
L4T1	1419.10	1388.10	1430.58	1432.08
L2T3	1496.80	1463.50	1495.31	0.10

Note: FEM = finite element method.

Table 3. Comparison of the frequency for a cylinder with closed and open ends.

Mode	FEM		BEM	
	Closed	Open	Closed	Open
L1	321.09	160.42	321.91	160.61
T1	587.80	609.30	596.48	614.59
L2	644.15	482.25	643.01	481.12
L1T1	669.79	760.31	665.61	755.50
L2T1	872.04	998.42	869.73	997.74
T2	976.78	990.83	974.74	980.14

Note: FEM = finite element method; BEM = boundary element method.

Laudien et al., 1995; Wieber, 1966) is presented in Table 2. It should be noted that there is a slight difference, of less than 1.5%, between the present model, the FEM and the literature for the corresponding modes, and 3% L^2 error norm percentage, which confirms the current formulation and the code developed based on it.

The results of a cylindrical chamber with an open-end condition are given in Table 3 and are compared with those of previous studies. The computations show a maximum of 1% difference for the corresponding modes and overall 1.5 L^2 error norm percentages between FEM and BEM in open cylinders. Besides, it can be evaluated that there is a maximum variation of 50% between open and closed cylinders, which can be detected for the first mode. An overall L^2 error norm of 59.61% between open and closed cylinders is computed.

The corresponding acoustic mode shapes of open and closed chambers are shown in Figure 2 for the first six frequencies. In the mode shape figures, red and blue colors show qualitatively the maximum and minimum displacements, respectively. Variations in longitudinal modes are more significant than those in other modes, and these

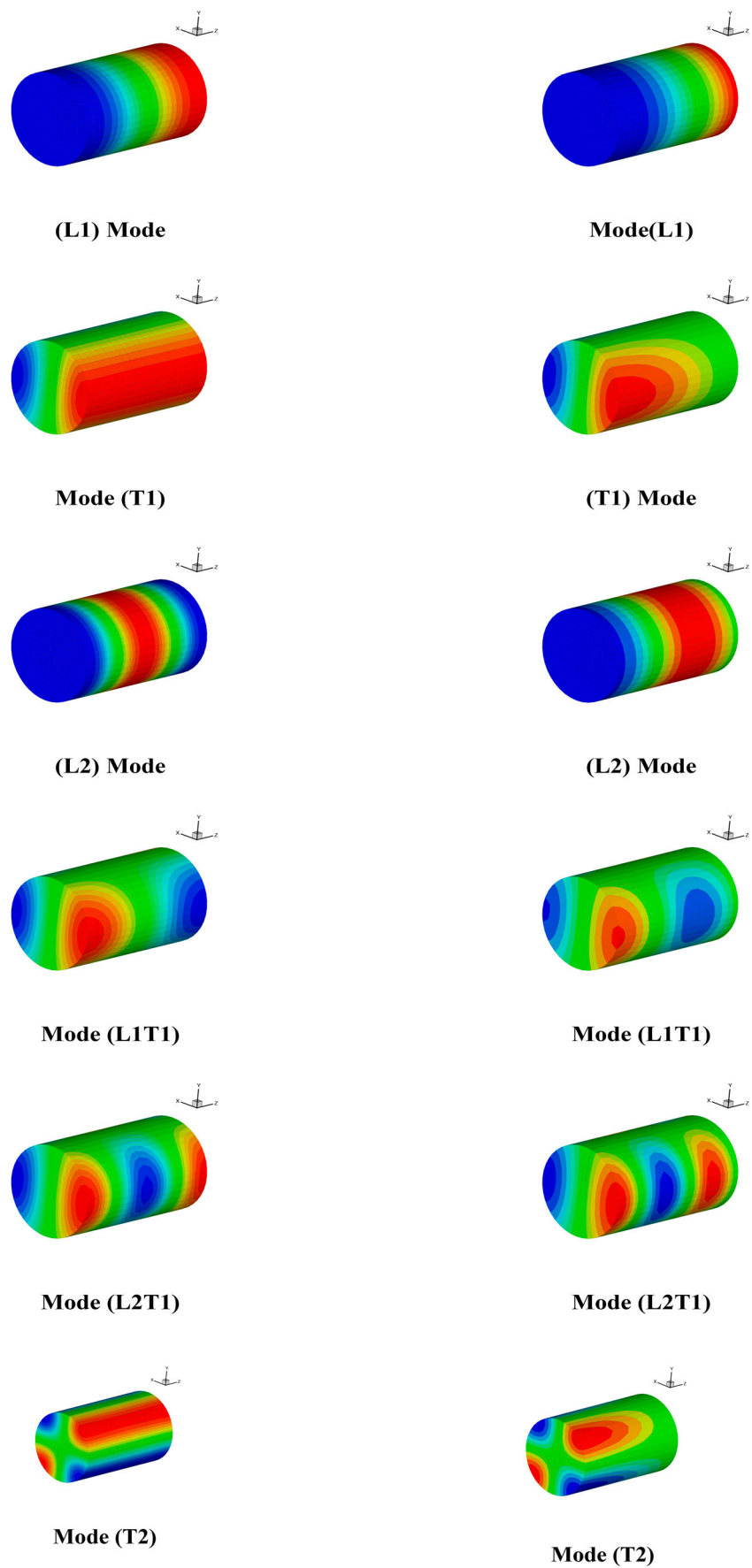


Figure 2. First three mode shapes of open and closed cylindrical chambers: (a) open end; (b) closed end.

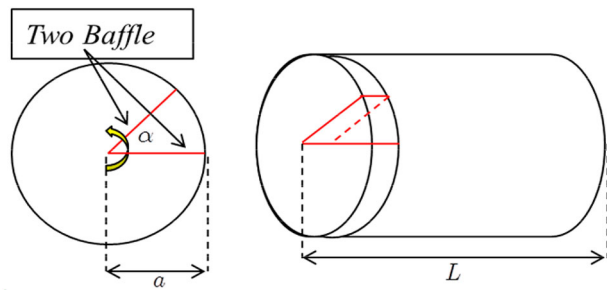


Figure 3. Typical configuration of a cylindrical chamber with two baffles.

modes in closed cylinders have greater values than those in open ones. The results also reveal that the open boundary condition has increasing effects on torsional and longitudinal–torsional frequencies.

5.2. Cylindrical chamber with radial baffles

A typical configuration of a cylindrical chamber with two baffles is shown in Figure 3.

To study the acoustic behavior of chambers with baffles, a second test case is considered as a cylindrical chamber with different radial baffle configurations. The frequencies of the acoustics with three, four and five baffles mounted radially at the inlet with 660 shell elements and 1320 nodes are given in Table 4. Letters T and L refer to modes in the tangential and longitudinal directions, respectively, and their index refers to the mode number. The baffles have a length of 30 mm. Results are extracted for an L/D ratio of 0.233 and show a 7.7–10.7% reduction in the first frequency for arrangements with four to six baffles, respectively.

Based on a mesh sensitivity analysis of a cylinder cavity with radial baffles and the literature (Farshchi et al., 2009; Laudien et al., 1995; Wieber, 1966), the accuracy of the numerical results is acceptable for $\frac{N_L}{N_B} = 0.22$. The slight difference between the current results and those in the literature can be inferred from the thickness of the baffles. The baffles significantly affect the circumferential and longitudinal–circumferential modes. It can be also concluded that the frequencies corresponding to L1T1 mode tend to disappear with an increasing number of baffles.

In addition, the influence of the baffle length is more prominent than the number of baffles, especially on the first circumferential mode. The computations for a chamber with five baffles, with an L/D ratio of approximately 0.333, show a 24% reduction in the frequency for T1 mode, whereas the reduction for the corresponding frequency reported in Laudien et al. (1995) is about 23%. The effects of baffle angle in comparison to FEM soft-

Table 4. Acoustic frequencies of a cylindrical chamber with different baffle configurations.

Mode	No baffle			Three baffles		
	FEM	BEM	FEM	Farshchi et al. (2009)	BEM	
L1	321.09	322.02	321.07	322.30	322.00	
T1	587.80	598.08	554.38	532.20	551.35	
L2	644.15	641.09	644.15	644.10	640.96	
L1T1	669.79	665.01	640.37	636.50	641.52	
L2T1	872.04	867.95	838.46	829.50	829.42	
L3	971.19	972.84	971.49	965.00	970.57	
T2	976.78	974.74	931.51	929.00	951.67	

Mode	Four baffles			Five baffles		
	FEM	Farshchi et al. (2009)	BEM	FEM	Farshchi et al. (2009)	BEM
L1	321.07	322.30	322.29	321.07	322.30	322.38
T1	545.82	522.10	541.65	540.76	513.80	534.14
L2	644.15	644.10	641.06	644.15	644.10	641.02
L1T1	638.29	635.70	640.98	637.26	634.90	640.78
L2T1	845.66	839.90	835.86	846.19	840.80	835.91
L3	971.49	965.00	971.42	971.49	965.00	970.99
T2	752.23	698.80	747.27	776.44	717.40	772.25

Note: FEM = finite element method; BEM = boundary element method.

ware on the non-dimensional frequencies are indicated in Figures 4–6. It can be observed that the frequency differences between the two circumferential modes are more tangible at 180° . The length of the baffle is 53 cm, c is the speed of sound and α . Modes T1, L1T1 and L2T1 at both 180° and 360° configurations have reductions of about 9.7%, 3.7% and 5.3%, respectively. The mode shapes of baffled and unbaffled cylinders are illustrated in Figure 7.

5.3. Combustion chamber

The third case is a combustion chamber with a converging nozzle. The chamber consists of two parts, namely a cylindrical section and a converging section. The length (L_c) of the cylinder section is 11 cm and the diameter (D_c) is 34 cm. The nozzle section has a length (L_n) of 42 cm and a 12 cm outlet diameter (D_n). The grid of the domain is constructed by shell elements (20 elements in the longitudinal direction, seven elements in the radial direction and 40 elements in the circumferential direction) (Figure 8).

The boundary conditions considered for the walls and opening are the same as those in the previous test case. Employing Newman boundary conditions at the inlet and outlet indicates differences in the pressure contours at the inlet and converged areas. Indeed, mode shapes of the nozzle depict a concentration in the pressure gradient at the throat area (Figure 9). A mesh study of the nozzle cavity is conducted for the first six frequencies

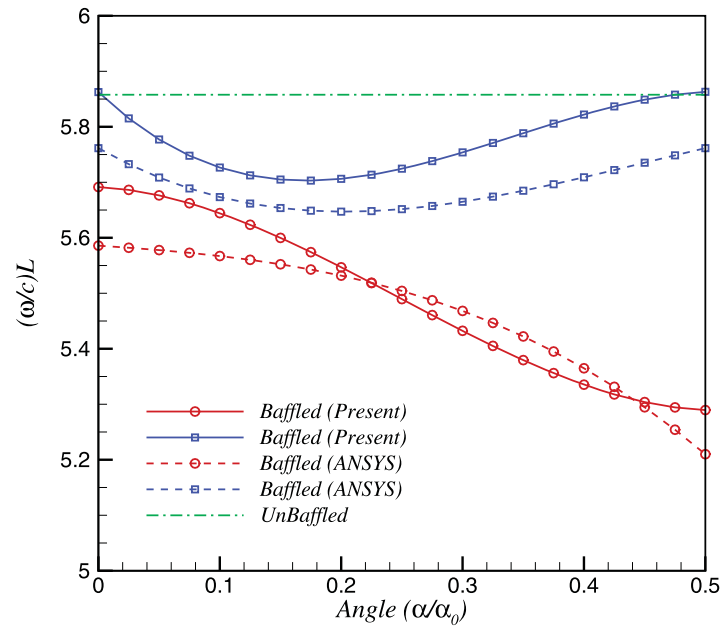


Figure 4. Non-dimensional form of T1 vs angle between two baffles.

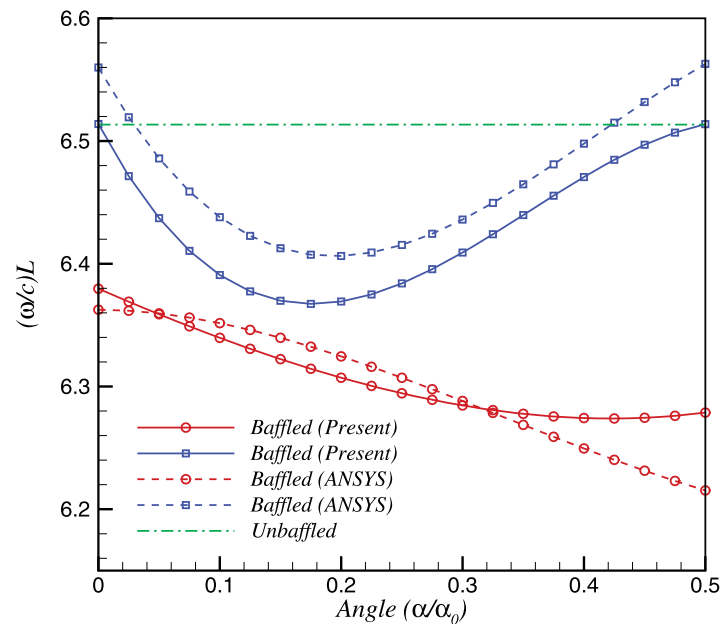


Figure 5. Non-dimensional form of L1T1 vs angle between two baffles.

using results from the literature (Farshchi et al., 2009; Laudien et al., 1995; Wieber, 1966) and the FEM, and the accuracy of numerical results is obtained for $\frac{N_I}{N_B} = 0.21$. An evaluation of natural frequencies for the closed-end nozzle shows negligible differences between the current model and the literature (Table 5). Moreover, the frequency of a nozzle chamber has a higher value than that of a cylindrical one. This can be inferred from the effective length and volume reduction in nozzle topology.

The first four natural frequencies for the closed-end combustion chamber reveal a significant decrease in longitudinal mode compared to those for the open-end chamber (Table 6).

Maximum variations of 73% for the corresponding modes, an overall error norm (L^2) of 83% between the open and closed chambers in the longitudinal direction, and near equality of both frequencies in the circumferential mode are found.

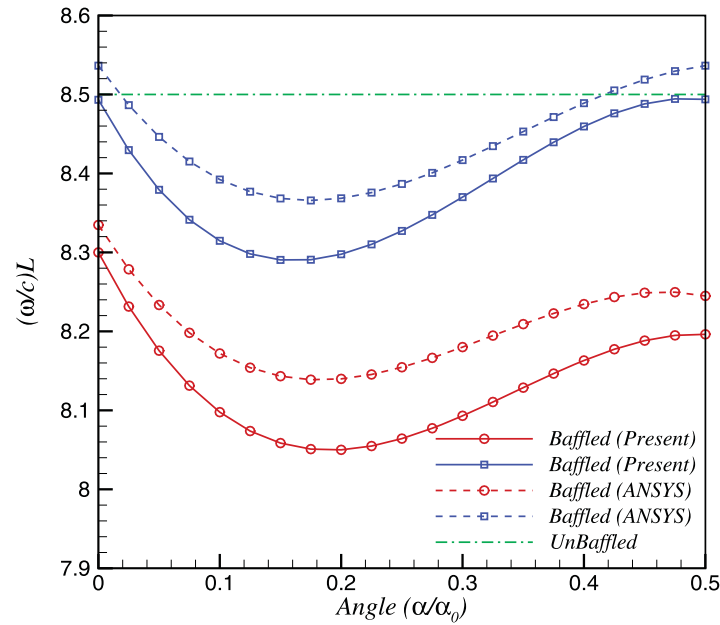


Figure 6. Non-dimensional form of L2T1 vs angle between two baffles.

Table 5. Combustion chamber frequencies.

Mode	Combustion		
	FEM	Farshchi et al. (2009)	BEM
L1	362.31	385.50	363.11
T1	632.40	660.50	641.64
L2	667.06	695.30	665.70
L1T1	937.82	979.60	933.56
L3	975.24	1007.90	982.73
T2	1017.13	1055.90	1009.11

Note: FEM = finite element method; BEM = boundary element method.

Table 6. Frequencies of closed- and open-end combustion chambers.

Mode	FEM		BEM	
	Closed	Open	Closed	Open
L1	362.31	96.40	363.11	96.41
T1	632.40	632.41	641.64	641.91
L2	667.06	469.54	665.70	468.90
L1T1	937.82	938.22	933.52	933.15
L3	975.24	793.86	982.73	794.58
T2	1017.13	1017.10	1009.11	1009.11

Note: FEM = finite element method; BEM = boundary element method.

5.4. Elastic converging nozzle with elastic baffle

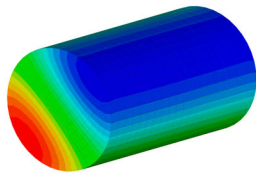
The effects of nozzle flexibility in the combustion chamber on acoustic frequencies are investigated in this example. The chamber is considered as a cantilever body with aluminum of 2024 material properties ($\rho_s = 2700 \text{ kg/m}^3$, $\nu = 0.3$ and $E = 71 \text{ GPa}$) at environmental temperature. Modal characteristics of the coupled system are evaluated using an efficient DRBEM/FEM based on the ROM formulation with 5700 shell elements and 22,400 nodes. The first 10 natural frequencies of the

Table 7. Frequencies of converged nozzle with elastic walls.

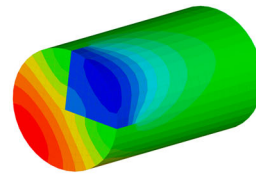
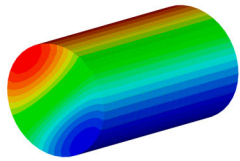
Mode	$t = 2 \text{ mm}$			$t = 5.5 \text{ mm}$		
	Structure	Acoustic	Coupled	Structure	Acoustic	Coupled
1	—	363.11	363.11	—	363.11	363.11
2	—	641.64	641.64	—	641.64	641.64
3	—	641.77	641.77	—	641.77	641.77
4	—	665.70	665.70	—	665.70	665.70
5	681.76	—	680.35	—	933.52	933.52
6	681.76	—	680.35	—	933.56	933.56
7	—	933.52	933.52	936.65	—	936.50
8	—	933.56	933.56	936.65	—	936.50
9	—	982.73	982.73	—	982.73	982.73
10	—	1009.11	1008.97	—	1009.11	1009.21

coupled domain are extracted using the lowest four mode shapes of individual acoustic and structure subdomains. Table 7 presents the coupled acoustoelastic frequencies for both 2 and 5 mm thicknesses. Frequencies of the structure at lower wall stiffness have a greater effect on the coupled domain.

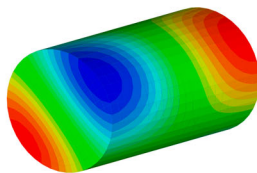
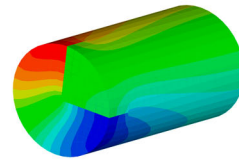
As a result of the coupling effect, structure frequencies decrease by 0.3% and acoustic frequencies increase by 0.4% for every mode. Besides, based on the results of the baffled cavity, the elasticity of the baffles highlights their coupling effects in circumferential and longitudinal–circumferential modes. Figure 10 illustrates the effect of the flexibility parameter ($\frac{\omega_a}{c}L$) versus the non-dimensional thickness ($\frac{t}{D}$) for acoustic dominant frequencies, where t is the thickness, c is the speed of sound, L is the length and D is the diameter of the cavity. It can be deduced that there is a coupling between acoustics and structure in high structural flexibility. In low non-dimensional thickness of structures, the results



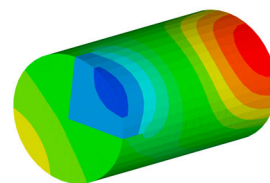
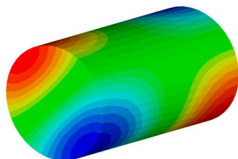
(a) T1 un-baffled shape Mode



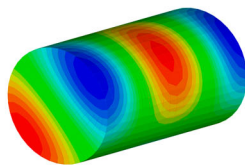
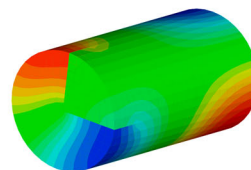
(b) T1 baffled shape Mode



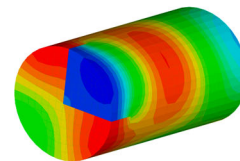
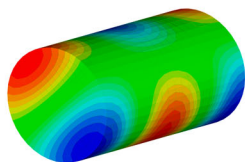
(c) L1T1 un-baffled shape Mode



(d) L1T1 baffled shape Mode



(e) L2T1 un-baffled shape Mode



(f) L2T1 baffled shape Mode

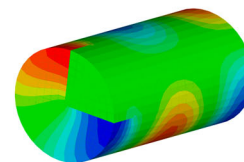


Figure 7. Shape modes of baffled and unbaffled cylinders: (a) T1 unbaffled; (b) T1 baffled; (c) L1T1 unbaffled; (d) L1T1 baffled; (e) L2T1 unbaffled; (f) L2T1 baffled.

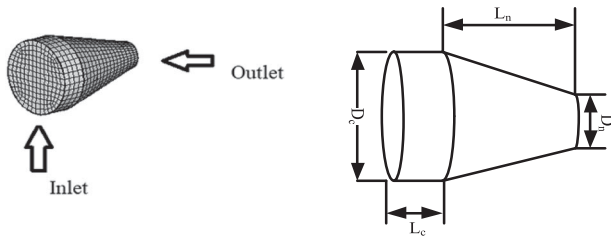


Figure 8. Nozzle chamber boundary mesh.

show that the first mode becomes stiff owing to coupling effects. The results also demonstrate a remarkable coupling system in L1T1 with the second mode of structures. Decreases in the structural and acoustic frequencies of 2.7% and 2.6%, respectively, are approximated.

5.5. Elastic axisymmetric tank

In this example, acoustic–structure characteristics of a symmetric tank are studied. Tanks are used extensively in pressure vessel industries. As can be seen, an axisymmetric boundary condition can be utilized for this case, where a tank is clamped along its central circumference. The geometry and boundary element mesh with 700 shell elements and 2790 nodes are illustrated in Figure 11. Studies with an emphasis on the vibration of a structure in the presence of an acoustic medium are conducted. The tank is constructed of steel alloy ($\rho_s = 8000 \text{ kg/m}^3$, $\nu = 0.3$ and $E = 210 \text{ GPa}$) with a thickness of 0.05 m and filled with a compressible fluid ($\rho_f = 565 \text{ kg/m}^3$ and $c = 730 \text{ m/s}$).

Following the above mesh study approach, the value $\frac{N_I}{N_B} = 0.21$ is used for the axisymmetric tank. The first

Table 8. First 10 frequencies of an elastic axisymmetric tank with uncoupled and coupled boundary conditions.

Mode	Uncoupled		Coupled	
	Structure	Acoustic	FEM	Present (ROM)
1	—	167.43	165.99	167.43
2	363.29	—	311.76	316.68
3	363.29	—	311.76	316.68
4	363.29	—	316.37	319.32
5	363.29	—	316.37	319.32
6	—	330.88	326.31	330.88
7	—	444.55	473.66	477.72
8	—	444.55	473.66	477.72
9	—	487.47	472.93	487.58
10	—	487.47	540.84	543.14

Note: FEM = finite element method; ROM = reduced-order method.

Table 9. First five frequencies of an elastic submerged submarine.

Mode	Stiffener number = 0		Stiffener number = 12	
	Jin et al. (2018)	Present (ROM)	Jin et al. (2018)	Present (ROM)
1	5	5.02	5	5.01
2	19	18.98	25	24.98
3	47	46.55	54.25	54.248
4	78	77.95	58.88	58.89
5	97	96.7	88.56	88.5

Note: ROM = reduced-order method.

10 coupled frequencies of the proposed FSI problem are listed in Table 8 and compared with the numerical results obtained from the FEM-based approach.

The lowest six modes of the structure without fluid for harmonic index 1 and the first 40 modes of the acoustic cavity are used in the ROM. The results demonstrate close values between the complete FEM-based results and reduced-order formulation results for the corresponding

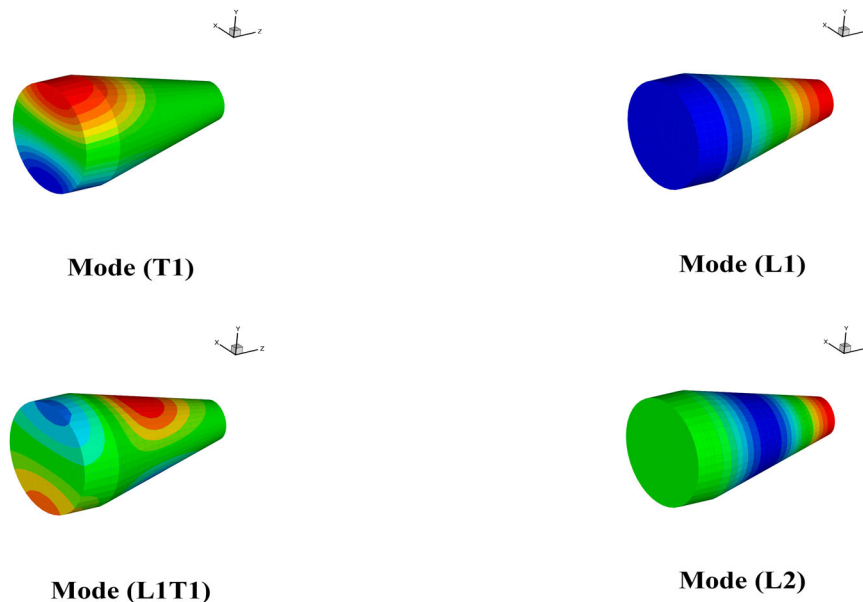


Figure 9. First four mode shapes of the closed-end nozzle chamber.

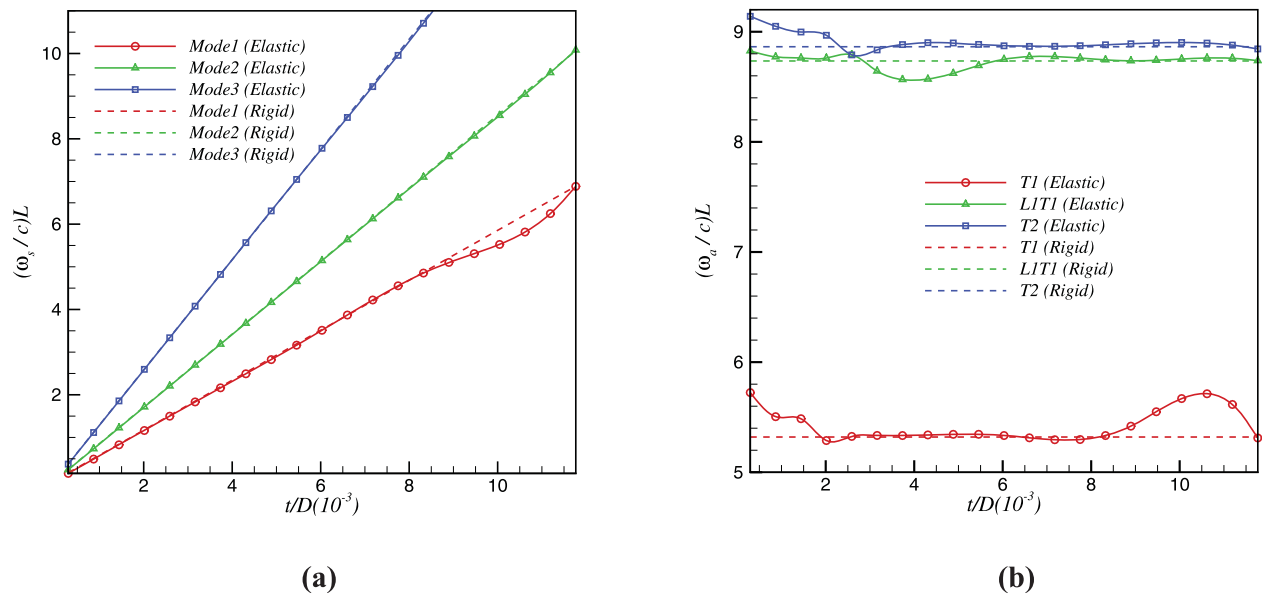


Figure 10. Variations of dimensionless coupled and uncoupled frequencies vs dimensionless thickness of elastic baffles in the nozzle cavity: (a) structure dominant frequencies; (b) acoustic dominant frequencies.

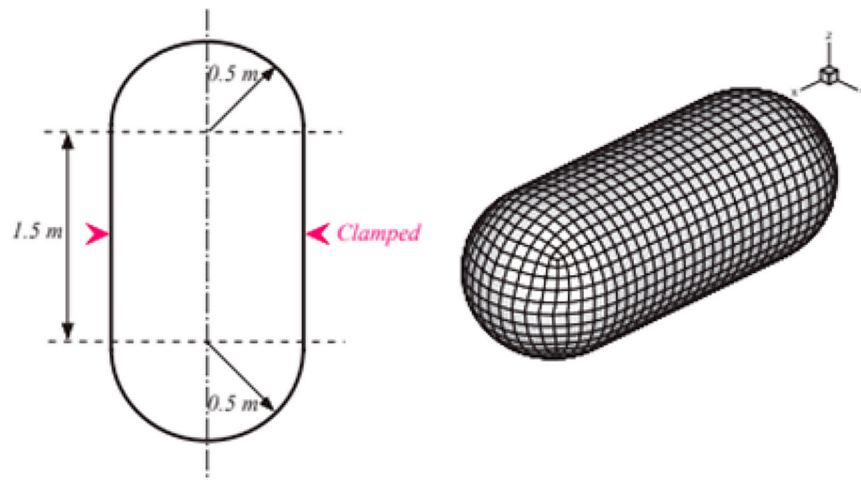


Figure 11. Geometry and boundary element mesh of an acoustic fluid in an elastic axisymmetric tank.

modes. As can be seen, the structure dominant frequencies decrease owing to the fluid effect. The mode shapes in mode 2 (structural dominant) and in mode 7 (acoustic dominant) are shown in Figure 12. It can be observed that the modes in the coupled system change significantly and are a combination of the corresponding mode shapes before coupling. In addition, because of the fluid, the coupling of the structure and acoustic medium becomes strong and the fluid influences the structure. Therefore, the structure is deflected and the structural mode shapes combine together via coupling, even in acoustic dominant modes. Consequently, it can be concluded that the vibration characteristics and the response of the structure change considerably as a result of fluid–structure interaction.

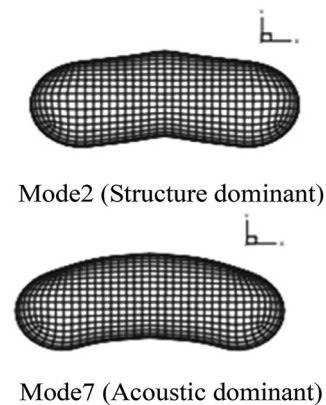


Figure 12. Structure mode shapes of the pressurized tank.

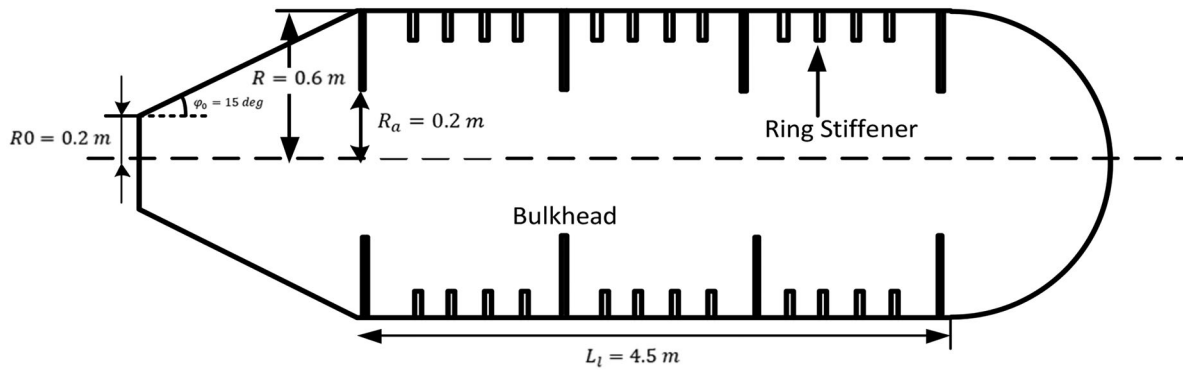


Figure 13. Schematic view of the submarine structure.

5.6. Elastic submarine with stiffener and bulkhead

The last test case is a submarine with a hull structure (Jin et al., 2018), which consists of a hemispherical truncated canonical-cylindrical steel shell with 8 mm thickness (Figure 13). The structure is reinforced with eight bulkheads and several ring stiffeners. Evaluations are conducted for steel alloy ($\rho_s = 7800 \text{ kg/m}^3$, $\nu = 0.3$ and $E = 210 \text{ GPa}$) filled with air ($\rho_{air} = 1.29 \text{ kg/m}^3$, $c_{air} = 340 \text{ m/s}$) and submerged in water ($\rho_{water} = 1000 \text{ kg/m}^3$, $c_{water} = 1500 \text{ m/s}$).

Here, the number of stiffeners and their effects on the dynamic behavior of the submerged submarine structure are investigated with 6000 shell elements and 23,950 nodes. The first five modes of the structure and the first five acoustic modes with $\frac{N_L}{N_B} = 0.2$ are applied to utilize the ROM form of the coupled formulation. Comparison of the first five coupled frequencies for zero and 12 stiffeners with those in the literature shows good agreement between the results.

It should be emphasized that there is a slight difference, of less than 1%, between the present model and the literature for the corresponding modes. Furthermore, it can be observed that the rings increase the first three frequencies and decrease for the third and fourth frequencies of the coupled systems. Results on vibrational characteristics reveal that the response of the structure changes considerably owing to fluid-structure interaction in higher modes.

Conclusions

Acoustic-structure interactions in chambers comprising rigid/elastic baffles and elastic walls are investigated with a novel FEM-BEM formulation in this article. The governing equations of the acoustic and structure domains are introduced, based on the BEM and FEM. Afterwards, the reduced-order model of the coupled system

with baffled and unbaffled chambers is derived using a modal analysis technique. The proposed formulation is examined by comparing the results with the literature, and the effects of baffles and elasticity of the walls are studied through a comprehensive study.

The results generally confirm the accuracy of the proposed formulation. Comparison of the results with those reported in the literature and the FEM shows that there is good agreement between them. Considering baffles in the chamber construction generally leads to a considerable reduction of acoustic frequencies. The results indicate that an optimum value can be found for acoustic frequencies of a chamber with two radial baffles by changing the angular position of the baffles. It can be inferred that the converging nozzle section of a combustion chamber transforms pure longitudinal modes into the radial direction and pure tangential modes into the longitudinal direction. Furthermore, this study demonstrates that by considering the elasticity of the nozzle section of a combustor, no coupling occurs in the structure and acoustic mode shapes even if the natural frequencies of the structure and the acoustic domains approach each other. Therefore, it can be inferred that the elasticity of a nozzle has a negligible influence on the acoustic characteristics of the combustor. The averaged error of less than 2% proves the capability of the proposed approach in the coupled analysis of acoustic problems. However, the last case study, on an axisymmetric and elastic submarine, shows high coupling between the acoustics and the structure. In this paper, the main limitation is the application of the proposed formulation to linear acoustic-structure cavity problems with rigid and elastic baffles. Nonlinear fluid-structure acoustic problems with complex structures could be developed in the future. The overall CPU time for acoustic mode evaluation based on the FEM computation is about 30% longer than that of the reduced-order BEM-based formulation.

Disclosure statement

No potential conflict of interest was reported by the authors.

Funding

This work was sponsored by the philosophy and social science planing project of Guangdong province [grant no. gd20ygl12], basic and applied basic project of Guangzhou city [grant no. 202102020629], Philosophy and social science planning project of Guangzhou city [grant no. 2121GZGJ48].

ORCID

Shahab S. Band  <http://orcid.org/0000-0001-6109-1311>

Kwok-wing Chau  <http://orcid.org/0000-0001-6457-161X>

References

- Ali, A., Rajakumar, C., & Yunus, S. M. (1995). Advances in acoustic eigenvalue analysis using boundary element method. *Computers & Structures*, 56(5), 837–847. [https://doi.org/10.1016/0045-7949\(95\)00012-6](https://doi.org/10.1016/0045-7949(95)00012-6)
- Anderson, W. E., & Yang, V. (1995). *Liquid rocket engine combustion instability*. American Institute of Aeronautics and Astronautics.
- Ar'kov, O. F., Voitsekhovskii, B. V., Mitrofanov, V. V., & Topchiyan, M. E. (1972). On the spinning-detonation-like properties of high frequency tangential oscillations in combustion chambers of liquid fuel rocket engines. *Journal of Applied Mechanics and Technical Physics*, 11(1), 159–161. <https://doi.org/10.1007/BF01102693>
- Atalla, N., & Bernhard, R. J. (1994). Review of numerical solutions for low-frequency structural-acoustic problems. *Applied Acoustics*, 43(3), 271–294. [https://doi.org/10.1016/003-682X\(94\)90050-7](https://doi.org/10.1016/003-682X(94)90050-7)
- Baer, M. R., & Mitchell, C. E. (1977). Theoretical evaluation of rigid baffles in suppression of combustion instability. *AIAA Journal*, 15(2), 135–136. <https://doi.org/10.2514/3.60613>
- Brebbia, C. A., & Dominguez, J. (1994). *Boundary elements: An introductory course*. WIT press.
- Brebbia, C. A., & Dominguez, J. (1994). *Boundary elements: An introductory course*. WIT press.
- Chen, L., Gao, Y., Wang, D., Zou, Q., & Zhang, S. (2020). Numerical simulation on acoustic mode and pressure-oscillation decay in finocyl-and axil-grain combustion chambers. *Aerospace Science and Technology*, 107, 106351. <https://doi.org/10.1016/j.ast.2020.106351>
- Chen, L. L., Lian, H., Liu, Z., Chen, H. B., Atroshchenko, E., & Bordas, S. P. A. (2019). Structural shape optimization of three dimensional acoustic problems with isogeometric boundary element methods. *Computer Methods in Applied Mechanics and Engineering*, 355, 926–951. <https://doi.org/10.1016/j.cma.2019.06.012>
- Craggs, A. (1972). The use of simple three-dimensional acoustic finite elements for determining the natural modes and frequencies of complex shaped enclosures. *Journal of Sound and Vibration*, 23(3), 331–339. [https://doi.org/10.1016/0022-460X\(72\)90629-3](https://doi.org/10.1016/0022-460X(72)90629-3)
- Dölz, J., Harbrecht, H., Kurz, S., Schöps, S., & Wolf, F. (2018). A fast isogeometric BEM for the three dimensional laplace-and Helmholtz problems. *Computer Methods in Applied Mechanics and Engineering*, 330, 83–101. <https://doi.org/10.1016/j.cma.2017.10.020>
- Fahmy, M. A. (2018). Shape design sensitivity and optimization for two-temperature generalized magneto-thermoelastic problems using time-domain DRBEM. *Journal of Thermal Stresses*, 41(1), 119–138. <https://doi.org/10.1080/01495739.2017.1387880>
- Farshchi, M., Mehrjou, H., & Salehi, M. M. (2009). Acoustic characteristics of a rocket combustion chamber: Radial baffle effects. *Applied Acoustics*, 70(8), 1051–1060. <https://doi.org/10.1016/j.apacoust.2009.03.001>
- Firouz-Abadi, R. D., Haddadpour, H., Noorian, M. A., & Ghasemi, M. (2008). A 3D BEM model for liquid sloshing in baffled tanks. *International Journal for Numerical Methods in Engineering*, 76(9), 1419–1433. <https://doi.org/10.1002/nme.2363>
- Gaul, L., & Wenzel, W. (2002). A coupled symmetric BE–FE method for acoustic fluid–structure interaction. *Engineering Analysis with Boundary Elements*, 26(7), 629–636. [https://doi.org/10.1016/S0955-7997\(02\)00020-6](https://doi.org/10.1016/S0955-7997(02)00020-6)
- Ghalandari, M., Bornassi, S., Shamshirband, S., Mosavi, A., & Chau, K. W. (2019). Investigation of submerged structures' flexibility on sloshing frequency using a boundary element method and finite element analysis. *Engineering Applications of Computational Fluid Mechanics*, 13(1), 519–528. <https://doi.org/10.1080/19942060.2019.1619197>
- Ghalandari, M., Shamshirband, S., Mosavi, A., & Chau, K. (2019). Flutter speed estimation using presented differential quadrature method formulation. *Engineering Applications of Computational Fluid Mechanics*, 13(1), 804–810. <https://doi.org/10.1080/19942060.2019.1627676>
- Ghalandari, M., Ziamolki, A., Mosavi, A., Shamshirband, S., Chau, K.-W., & Bornassi, S. (2019). Aeromechanical optimization of first row compressor test stand blades using a hybrid machine learning model of genetic algorithm, artificial neural networks and design of experiments. *Engineering Applications of Computational Fluid Mechanics*, 13(1), 892–904. <https://doi.org/10.1080/19942060.2019.1649196>
- Gladwell, G. M. L., & Zimmermann, G. (1966). On energy and complementary energy formulations of acoustic and structural vibration problems. *Journal of Sound and Vibration*, 3(3), 233–241. [https://doi.org/10.1016/0022-460X\(66\)90092-7](https://doi.org/10.1016/0022-460X(66)90092-7)
- Gonzalez-Flesca, M., Scoufflaire, P., Schmitt, T., Ducruix, S., Candel, S., & Mery, Y. (2018). Reduced order modeling approach to combustion instabilities of liquid rocket engines. *AIAA Journal*, 56(12), 4845–4857. <https://doi.org/10.2514/1.J057098>
- Hambric, S. A., Sung, S. H., & Nefske, D. J. (2016). *Engineering vibroacoustic analysis: Methods and applications*. John Wiley & Sons.
- Han, L., Li, J., Zhao, D., Gu, X., Ma, B., & Wang, N. (2021). Effects of baffle designs on damping acoustic oscillations in a solid rocket motor. *Aerospace Science and Technology*, 106827. <https://doi.org/10.1016/j.ast.2021.106827>
- Hussin, A. E., Hamed, A. M., Kamal, M. M., & Elbaz, A. R. (2021). Development of an industrial burner accommodating methane-Air triple flames. *Combustion Science and Technology*, 193(1), 23–39. <https://doi.org/10.1080/00102202.2019.1649665>

- Iurashev, D., Campa, G., Anisimov, V. V., & Cosatto, E. (2017). Two-step approach for pressure oscillations prediction in gas turbine combustion chambers. *International Journal of Spray and Combustion Dynamics*, 9(4), 424–437. <https://doi.org/10.1177/1756827717711016>
- Jin, G., Ma, X., Wang, W., & Liu, Z. (2018). An energy-based formulation for vibro-acoustic analysis of submerged submarine hull structures. *Ocean Engineering*, 164, 402–413. <https://doi.org/10.1016/j.oceaneng.2018.06.057>
- Junge, M., Brunner, D., & Gaul, L. (2011). Solution of FE-BE coupled eigenvalue problems for the prediction of the vibro-acoustic behavior of ship-like structures. *International Journal for Numerical Methods in Engineering*, 87(7), 664–676. <https://doi.org/10.1002/nme.3124>
- Kamiya, N., Andoh, E., & Nogae, K. (1993). Eigenvalue analysis by the boundary element method: New developments. *Engineering Analysis with Boundary Elements*, 12(3), 151–162. [https://doi.org/10.1016/0955-7997\(93\)90011-9](https://doi.org/10.1016/0955-7997(93)90011-9)
- Kim, S.-K., Choi, H. S., Kim, H. J., Ko, Y. S., & Sohn, C. H. (2015). Finite element analysis for acoustic characteristics of combustion stabilization devices. *Aerospace Science and Technology*, 42, 229–240. <https://doi.org/10.1016/j.ast.2015.01.024>
- Kontoni, D. P. N., Partridge, P. W., & Brebbia, C. A. (1991). The dual reciprocity boundary element method for the eigenvalue analysis of Helmholtz problems. *Advances in Engineering Software and Workstations*, 13(1), 2–16. [https://doi.org/10.1016/0961-3552\(91\)90040-B](https://doi.org/10.1016/0961-3552(91)90040-B)
- Laudien, E., Pongratz, R., Pierro, R., & Preclik, D. (1995). Experimental procedures aiding the design of acoustic cavities. *Progress in Astronautics and Aeronautics*, 169, 377–402.
- Li, J., Wang, D., Morgans, A. S., & Yang, L. (2021). Analytical solutions of acoustic field in annular combustion chambers with non-uniform cross-sectional surface area and mean flow. *Journal of Sound and Vibration*, 506, 116175. <https://doi.org/10.1016/j.jsv.2021.116175>
- Ohayon, R. (2001). Reduced symmetric models for modal analysis of internal structural-acoustic and hydroelastic-sloshing systems. *Computer Methods in Applied Mechanics and Engineering*, 190(24–25), 3009–3019. [https://doi.org/10.1016/S0045-7825\(00\)00379-0](https://doi.org/10.1016/S0045-7825(00)00379-0)
- Ohayon, R., & Soize, C. (2012). Advanced computational dissipative structural acoustics and fluid-structure interaction in low-and medium-frequency domains. Reduced-order models and uncertainty quantification. *International Journal of Aeronautical and Space Sciences*, 13(2), 127–153. doi:10.5139/IJASS.2012.13.2.127
- Shu, G., Dong, L., & Liang, X. (2012). A review of experimental studies on deposits in the combustion chambers of internal combustion engines. *International Journal of Engine Research*, 13(4), 357–369. <https://doi.org/10.1177/146808741427661>
- Simpson, R. N., Scott, M. A., Taus, M., Thomas, D. C., & Lian, H. (2014). Acoustic isogeometric boundary element analysis. *Computer Methods in Applied Mechanics and Engineering*, 269, 265–290. <https://doi.org/10.1016/j.cma.2013.10.026>
- Sladek, V., Sladek, J., & Tanaka, M. (1993). Eigenvalue analysis of three-dimensional Helmholtz equation. *Engineering Analysis with Boundary Elements*, 11(2), 165–170. [https://doi.org/10.1016/0955-7997\(93\)90036-K](https://doi.org/10.1016/0955-7997(93)90036-K)
- Sui, C., Zhang, J., Zhang, L., Hu, X., & Zhang, B. (2021). Large eddy simulation of premixed hydrogen-rich gas turbine combustion based on reduced reaction mechanisms. *Engineering Applications of Computational Fluid Mechanics*, 15(1), 798–814. <https://doi.org/10.1080/19942060.2021.1918581>
- Webster, S., Hardi, J., & Oschwald, M. (2017). Measurement of acoustic dissipation in an experimental combustor under representative conditions. *Journal of Sound and Vibration*, 390, 39–54. <https://doi.org/10.1016/j.jsv.2016.11.032>
- Wieber, P. R. (1966). *Acoustic decay coefficients of simulated rocket combustors*. NASA.
- Wolf, J. A., Jr. (1976). Modal synthesis for combined structural-acoustic systems. *AIAA Journal*, 14(1), 33–38. <https://doi.org/10.2514/3.7363>
- Wu, Y. H., Dong, C. Y., & Yang, H. S. (2020). Isogeometric FE-BE coupling approach for structural-acoustic interaction. *Journal of Sound and Vibration*, 481, 115436. <https://doi.org/10.1016/j.jsv.2020.115436>
- Yu, B., Cao, G., Meng, Z., Gong, Y., & Dong, C. (2021). Three-dimensional transient heat conduction problems in FGMs via IG-DRBEM. *Computer Methods in Applied Mechanics and Engineering*, 384, 113958. <https://doi.org/10.1016/j.cma.2021.113958>
- Zeinalzadeh, A., & Pakatchian, M. R. (2021). Evaluation of novel-objective functions in the design optimization of a transonic rotor by using deep learning. *Engineering Applications of Computational Fluid Mechanics*, 15(1), 561–583. <https://doi.org/10.1080/19942060.2021.1895889>
- Zhao, D., & Li, X. Y. (2015). A review of acoustic dampers applied to combustion chambers in aerospace industry. *Progress in Aerospace Sciences*, 74, 114–130. <https://doi.org/10.1016/j.paerosci.2014.12.003>
- Zhao, W., Chen, L., Chen, H., & Marburg, S. (2019). Topology optimization of exterior acoustic-structure interaction systems using the coupled FEM-BEM method. *International Journal for Numerical Methods in Engineering*, 119(5), 404–431. doi:10.1002/nme.6055